nature physics

SUPPLEMENTARY INFORMATION

DOI: 10.1038/NPHYS3629

Double-Q spin-density wave in iron arsenide superconductors

THEORY OF C_4 MAGNETIC ORDER

In this supplementary section, we discuss why, in the non-uniform phase, the spins reorient and point out of the plane. The magnetic phase in most parent compounds of the iron-based superconductors is the stripe spin-density wave order with ordering vector $\mathbf{Q}_1 = (\pi, 0)$ or $\mathbf{Q}_2 = (0, \pi)$ in the unfolded Brillouin zone, in which there is one iron atom per unit cell. These two wave-vectors connect the hole pockets at the center of the Brillouin zone and the electron pockets at the zone boundary, along the two orthogonal iron-iron bond directions, as shown in Figure S1. The stripe magnetic ordering breaks both O(3) spin-rotational symmetry and C_4 lattice rotational symmetry (by selecting either $\mathbf{Q}_1$ or $\mathbf{Q}_2$), and is often preceded by a spin nematic phase in which C_4 symmetry is broken, but O(3) rotational symmetry remains unbroken [1]. Nevertheless, the Fermi surface geometry of iron pnictides allows double-$\mathbf{Q}$ tetragonal orders in which both $\mathbf{Q}_1$ and $\mathbf{Q}_2$ are present. The free energy expansion in terms of the two magnetic order parameters $\mathbf{M}_1$ and $\mathbf{M}_2$ (associated with the ordering vectors $\mathbf{Q}_1$ and $\mathbf{Q}_2$) captures these different possible ground states:

$$F_m(\mathbf{M}_i) = a\left(M_1^2 + M_2^2\right) + \frac{u}{2}\left(M_1^2 + M_2^2\right)^2 - \frac{g}{2}\left(M_1^2 - M_2^2\right)^2 + 2w\left(\mathbf{M}_1 \cdot \mathbf{M}_2\right)^2 \tag{1}$$

In particular, for $g > 0$ and $g > -w$, the ground state is the stripe phase, with $M_1 = 0$ or $M_2 = 0$. For $g < 0$ and $w < 0$ or $0 < g < -w$, the ground state is the tetragonal double-$\mathbf{Q}$ phase, $M_1^2 = M_2^2$, with $\mathbf{M}_1 \parallel \mathbf{M}_2$ (*i.e.*, the non-uniform phase) whereas for $g < 0$ and $w > 0$ the tetragonal double-$\mathbf{Q}$ state realized is a non-collinear one with $\mathbf{M}_1 \perp \mathbf{M}_2$. Microscopic calculations show different regimes in which both types of phases have the lowest energy [2–4].

In this model, the magnetic order parameter has $O(3)$ symmetry. However, in the actual system, there is magnetic anisotropy introduced by the on-site spin-orbit coupling, $\lambda \mathbf{S} \cdot \mathbf{L}$. Typically, in tetragonal symmetry, the spin-orbit coupling necessarily introduces either an easy axis or an easy plane anisotropy, enforcing the magnetic moments to point either in-plane or out-of plane. Thus, in general, one expects the free energy to acquire the additional quadratic term:

$$\tilde{F}_m(M_{i,a}) = \alpha_1\left(M_{1,x}^2 + M_{2,y}^2\right) + \alpha_2\left(M_{1,y}^2 + M_{2,x}^2\right) + \alpha_3\left(M_{1,z}^2 + M_{2,z}^2\right) \tag{2}$$

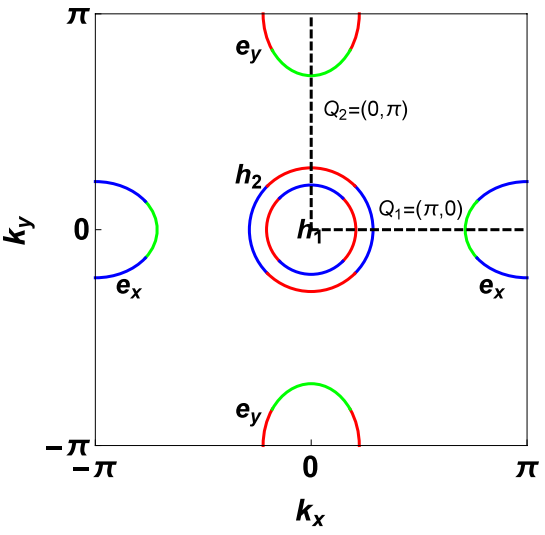

FIG. S1: Typical Fermi surface of the iron pnictides (h denotes hole pockets and e, electron pockets) in the Fe_2As_2 layer shown in the so-called single Fe-ion per unit cell Brillouine Zone. The orbital content of the Fermi surface is represented by various colors, namely, red denotes the d_{xz} orbital, blue, the d_{yz}orbital and green, the d_{xy}orbital.

DOI: 10.1038/NPHYS3629

The origin of these spin anisotropies traces back to the orbital character of the electronic Fermi surfaces, which places further constraints on the form of the free energy. In particular, note from Fig. S1 that the orbital content of the electron pocket centered at $(0,\pi)$ consists of a mixture of xy and xz orbitals, while the C_4-rotated electron pocket centered at the $(\pi,0)$ point is a mixture of xy and yz orbitals. Thus, the components $M_{1,x}$ and $M_{2,y}$, as well as $M_{1,y}$ and $M_{2,x}$, are related by a 90° rotation in the presence of spin-orbit coupling.

This reasoning can be rigorously justified using the group-theory arguments put forward in Ref. 5. The space-group symmetry of a single FeAs plane is *P4/nmm* due to the puckering of the As atom, which results in the doubling of the Fe unit cell. In this framework, the magnetic order parameters $\mathbf{M}_i$ must belong to the irreducible representations of this space group at the momentum $\mathbf{Q}_M = (\pi,\pi)$ (which corresponds to $\mathbf{Q}_1/\mathbf{Q}_2$ of the one-Fe Brillouin zone). As shown in Ref. 5, because of the non-symmorphic nature of the *P4/nmm* group, all of its irreducible representations at $\mathbf{Q}_M$ are two-dimensional. In real space, the only one that allows for a function peaked at the positions of the iron atoms is the so-called E_{M_4} representation. In the presence of spin-orbit coupling, this requirement restricts the possible orientations of $\mathbf{M}_i$. In particular, enforcing the orbital component of $\mathbf{M}_i$ to transform according to the E_{M_4} representation, there are three possible two-dimensional representations for $\mathbf{M}_i$:

$$E_{M_1}:\begin{pmatrix}M_{2,y}\\M_{1,x}\end{pmatrix}\qquad E_{M_2}:\begin{pmatrix}M_{2,x}\\M_{1,y}\end{pmatrix}\qquad E_{M_3}:\begin{pmatrix}M_{2,z}\\M_{1,z}\end{pmatrix} \tag{3}$$

Thus, each of these three different irreducible representations should have different transition temperatures, in agreement with Eq. (2). A straightforward analysis of this free energy reveals that there are only three possible spin configurations in the tetragonal double-**Q** phase:

- The magnetic order parameter $\mathbf{M}_1$ (with ordering vector $(\pi,0)$) points along the x axis, and $\mathbf{M}_2$ (with ordering vector $(0,\pi)$) points along the y axis. This corresponds to the non-collinear tetragonal configuration in which $\mathbf{M}_1 \perp \mathbf{M}_2$.
- $\mathbf{M}_1$ points along the y axis, and $\mathbf{M}_2$ points along the x axis. This also corresponds to another non-collinear configuration.
- Both $\mathbf{M}_1$ and $\mathbf{M}_2$ point along the z axis. This corresponds to a non-uniform configuration, in which $\mathbf{M}_1 \parallel \mathbf{M}_2$.

Therefore, the only spin orientation compatible with the non-uniform tetragonal state observed experimentally is an out-of-plane orientation, as also seen experimentally. Note that if α_3 is the smallest anisotropic coefficient, the system will develop non-uniform order immediately below T_N as long as $g < \max(0,-w)$.

In order for the non-uniform state to remain the ground state down to the lowest temperature, the quartic coefficients must satisfy the $g<0$, $w<0$ or $0<g<-w$ conditions. Within particular itinerant microscopic models, such a state was indeed found to be favoured over the stripe single-**Q** and non-collinear double-**Q** states over certain doping ranges [3, 4]. Here, we note that charge fluctuations can also favour this double-**Q** state over its non-collinear counterpart. In particular, due to the fact that, in one of the sublattices, the magnetization vanishes, the non-uniform state triggers an additional checkerboard charge order parameter, W, with wavevector $\mathbf{Q}_1+\mathbf{Q}_2=\mathbf{Q}_{ch}=(\pi,\pi)$. Fluctuations in this charge channel, in turn, introduce further corrections to the magnetic free energy. In particular, the free energy acquires the contribution [6]:

$$F_{ch} = \frac{1}{2}\chi_{ch}^{-1}(\mathbf{Q}_{ch})W^2 + \lambda W(\mathbf{M}_1\cdot\mathbf{M}_2) \tag{4}$$

where χ_{ch} is the charge susceptibility and λ, the coupling constant. Integrating out the charge degrees of freedom yields an effective correction to the magnetic free energy

$$F_m^{eff} = -\frac{1}{2}\lambda^2\chi_{ch}(\mathbf{Q}_{ch})(\mathbf{M}_1\cdot\mathbf{M}_2)^2 \tag{5}$$

which obviously favours $\mathbf{M}_1 \parallel \mathbf{M}_2$ rather than $\mathbf{M}_1 \perp \mathbf{M}_2$. In this regard, charge fluctuations can indeed support the experimentally observed state.

SAMPLE CHARACTERIZATION

The details of the sample preparation methods are given in the Methods section of the main article. The samples were synthesized in two batches with the nominal composition $Sr_{0.63}Na_{0.37}Fe_2As_2$ for x-ray diffraction (< 1 g) and

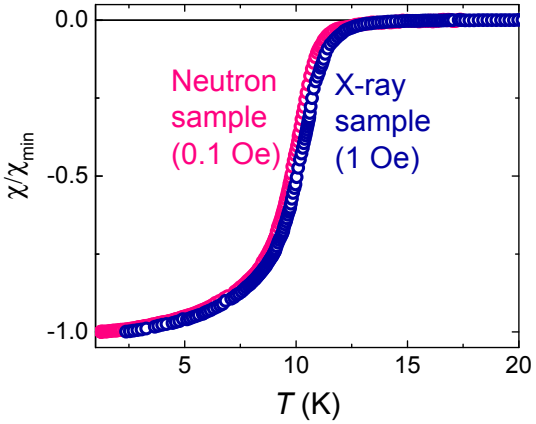

FIG. S2: Normalized magnetization of samples used for x-rays (blue curve) and neutrons (red curve) measured using a home-built SQUID magnetometer. Estimated superconducting volume fraction using the relation $4\pi\chi/\rho$ is well above 100%, suggesting bulk superconducting behavior.

neutron diffraction (4 g). Both had sharp superconducting transitions at $T_c = 12$ K (see Figure S2). The superconducting transitions are very sharp for a typical iron arsenide with the 122 structure and nearly equivalent in both compounds.

Rietveld refinements of x-ray powder diffraction yielded a composition of $x = 0.3691(5)$ in good agreement with the nominal stoichiometry. The temperature dependent lattice parameters of $Sr_{0.63}Na_{0.37}Fe_2As_2$ were determined from the x-ray diffraction experiments, and are shown in Figure S3. The c axis smoothly transforms while the thermal expansion of a axis changes sign at T_N and T_r. Occupancies of the Sr and Na sites were constrained to sum to one, and were refined independently in each scan. The average refined occupancy over all scans is $Occ_{Na} = 0.3691(5)$. This agrees well with the nominal composition $Sr_{0.63}Na_{0.37}Fe_2As_2$, so this is the name for the materials used throughout the paper.

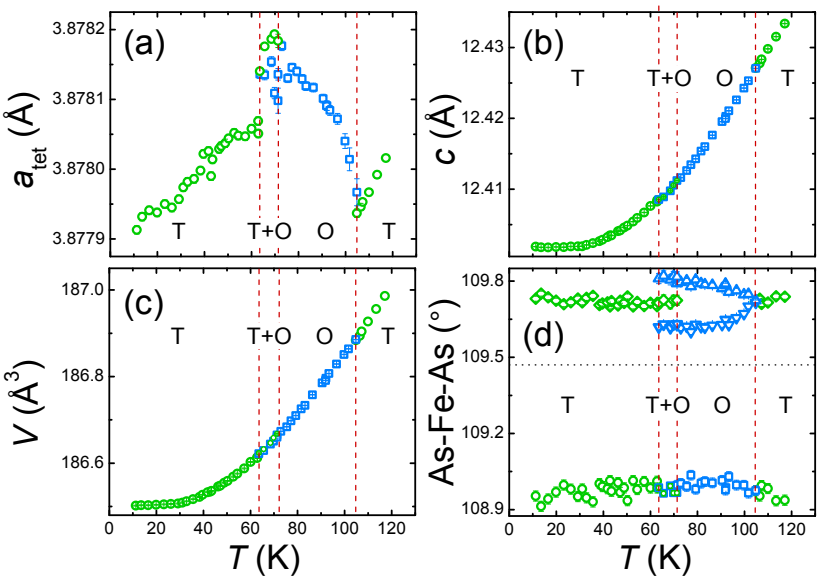

FIG. S3: Rietveld refinements results from the temperature dependent x-ray diffraction data of $Sr_{0.63}Na_{0.37}Fe_2As_2$ (11-BM). (a) is the primitive basal plane lattice spacing, a_{tet} (b) is the c axis, (c) is the cell volume, and (d) is the As-Fe-As bond angles. In (a-c), green circles depict the tetragonal phase and blue squares the orthorhombic one. In (d), the green circles and diamonds depict α_1 (the in-plane bond angle) and α_2 (the out-of-plane bond angle) of the tetragonal phase, respectively. Blue squares depict α_1 for the orthorhombic phase and blue up- and down-triangles each depict one of the two values taken by α_2 in the orthorhombically distorted cell.The temperature ranges of the tetragonal (T) and orthorhombic (O) phases are marked on each graph, and separated by dotted red lines.

DOI: 10.1038/NPHYS3629

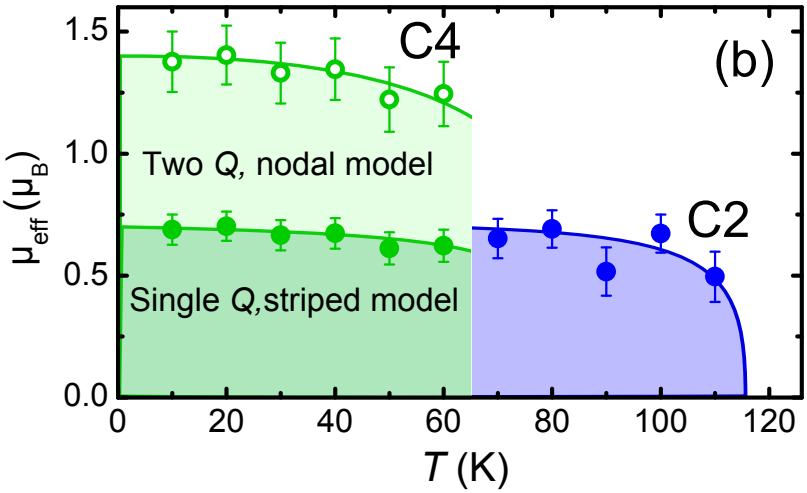

FIG. S4: The magnetic order parameter determined from Rietveld refinement of neutron diffraction measured on POWGEN at 10 K. Below $T_r \sim 65$ K, two interpretations are consistent with the diffraction analysis. The solid and open circles represent the magnetic moments on the magnetic iron sites assuming a two-domain C_2 stripe model and a single-domain C_4 model, respectively. The lines are guides to the eye. The error bars are determined by the standard deviation of the Rietveld refinement parameters.

We should note that the slight difference in the peak widths of the two orthorhombically split reflections shown in Fig. 1(b) of the manuscript is not caused by sample inhomogeneity. Sample inhomogeneity would give approximately equal broadening of each peak, since both the orthorhombic a and b parameters are known to change uniformly with composition in these hole-doped families, *e.g.*, see Ref. 7. The hole-doped 122 iron arsenides are relatively soft and susceptible to strain broadening, which can be modelled by anistropic strain parameters in the Rietveld refinement. We found a very slight (5%) increase in the (400) term over the (040), which means that the crystallites are more strongly strained along the longer orthorhombic lattice parameter.

MAGNETIC NEUTRON DIFFRACTION

The HFIR data shown in Fig. 1c of the manuscript show that the transition temperature of the C_2 phase in the neutron sample is $T_N \sim 115$ K, rather than the 105 K seen in the x-ray sample. Uncertainties in the background level of the paramagnetic phase make this value approximate, although it is consistent with Rietveld refinements of the neutron diffraction on POWGEN (Fig. S4). An example of such a refinement is shown in Fig. 1e. The C_4 transition, which is revealed by the growth in intensity of the $(\frac{1}{2}\frac{1}{2}1)$ peak (Fig. 1d), also occurs at the slightly lower temperature of 65 K (*cf* 73 K in the x-ray sample). The T_N value suggests that the stoichiometry is slightly lower than in the x-ray sample. Without more comprehensive measurements of the phase diagram, we cannot estimate the composition of the neutron sample more precisely, but we note that the sample used in the Mössbauer measurements was the same as the one used in the x-ray diffraction, and the transition temperatures are consistent in both techniques, so the discrepancy in the stoichiometries does not affect any of our conclusions.

Figure S4 shows the refined magnetization of the iron sites determined from Rietveld refinement of the POWGEN data. As stated in the main manuscript, it is not possible for diffraction to distinguish between a single-$\mathbf{Q}$ model, *i.e.*, $\mathbf{S}(\mathbf{r}) = \mathbf{M}_i \cos(\mathbf{Q}_i \cdot \mathbf{r})$, with domains of $\mathbf{Q}_1 = (\pi, 0)$ or $\mathbf{Q}_2 = (0, \pi)$ stripes, or a double-$\mathbf{Q}$ model formed by the coherent superposition of $\mathbf{Q}_1$ and $\mathbf{Q}_2$ modulations, *i.e.*, $\mathbf{S}(\mathbf{r}) = \mathbf{M}_1 \cos(\mathbf{Q}_1 \cdot \mathbf{r}) + \mathbf{M}_2 \cos(\mathbf{Q}_2 \cdot \mathbf{r})$. In both case, neutron diffraction yields M_1 $(= M_2)$. The moment on the magnetic iron sites are displayed in the figure, with the C_2 moments representing M_1 and the C_4 moments representing $M_1 + M_2$, *i.e.*, double the size of the C_2 moments.

MÖSSBAUER SPECTROSCOPY

Mössbauer spectra were measured at 5, 15, 30, 65, 75, 85, 95, 105, and 125 K using the same sample measured by x-ray diffraction. In each case, the spectra were fit using a non-linear least-squares program to parameters representing

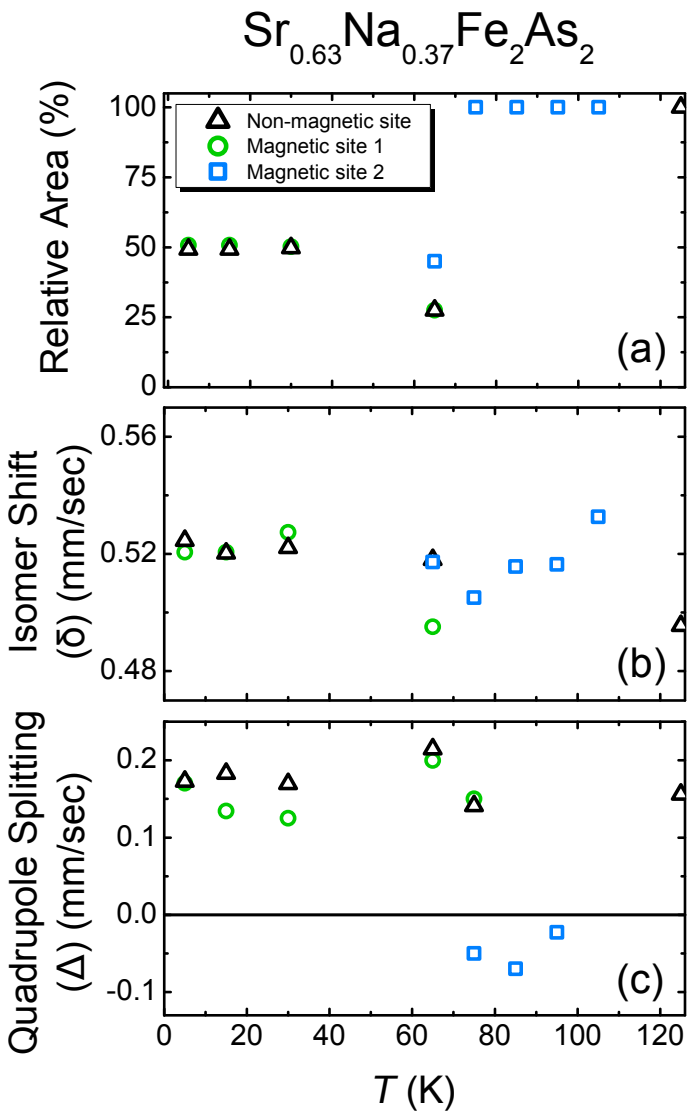

FIG. S5: Temperature dependent parameters from the fits to the Mössbauer data, with the non-magnetic site shown in black triangles, the low-temperature type magnetic site as green circles, and the high-temperature type magnetic site in blue squares. (a) The relative area, (b) the isomer shifts, and (c) the quadrupole splitting for each iron site.

the isomer shift, magnetic splitting, and the quadrupole splitting. The intensities of the magnetic sextet-split lines were constrained to a 1:2:3 ratio according to their Clebsch-Gordon coefficients, and the Lorentzian linewidths for all lines of a particular iron site were constrained to be the same. Selected spectra are shown in Fig. 3 of the main article.

Parameters relating to the fit models are shown in Figure S5. At most temperatures the plotted parameters were allowed to refine freely. At 125 K, *i.e.*, above $T_N = 105$ K, the spectrum was modelled by a single non-magnetic site. Between 105 and 75 K, the spectra in the C_2 phase were well fit to a single magnetic site, with a hyperfine field that grows with decreasing temperature. The quadrupole splitting reverses sign in this temperature range, presumably as a result of the structural transition to orthorhombic symmetry. At 30 K and below in the C_4 phase, the spectra required two sites, one non-magnetic and the other magnetic, with 50% volume fraction. The hyperfine field on the magnetic sites, shown in Fig. 3e of the main article, is approximately double the value in the C_2 phase at 75 K. We note that there is a slight decrease in the magnetic splitting at $T = 5$ K, *i.e.*, below $T_c = 12$ K, but it is too small to draw any strong conclusions about phase competition with superconductivity. In recently published results on K-doped $BaFe_2As_2$, Böhmer *et al* observe a complete suppression of the C_4 phase below the T_c in favour of the C_2 phase [8], but C_2 phase is not restored in either $(Ba,Na)Fe_2As_2$ [9, 10] or this sample. This presumably reflects the relative stability of the C_4 phase in each compound and is the subject of further investigation. The quadrupole

DOI: 10.1038/NPHYS3629

splitting switches sign again on both sites and is close to its value in the high-temperature tetragonal phase. The isomer shift does not vary significantly across the whole temperature range.

At 65 K, where the spectrum appears to be multicomponent, the parameters were too highly correlated to trust a completely free fit. Since the x-ray data indicated that both C_2 and C_4 phases were present at this temperature (see Fig. S3), the spectrum was assumed to be a superposition of the magnetic and non-magnetic sites from the C_4 phase with the magnetic site from the C_2 phase. The isomer shift and quadrupole splitting were held constant at the average value for each determined at other temperatures for each site, and only the relative area and effective magnetic field were allowed to refine. This gave a good match to the data and internally consistent values for the refined terms.

[1] R. M. Fernandes, A. V. Chubukov, J. Knolle, I. Eremin, and J. Schmalian, Phys. Rev. B **85**, 024534 (2012).
[2] I. Eremin and A. V. Chubukov, Phys. Rev. B **81**, 024511 (2010).
[3] X. Wang and R. M. Fernandes, Phys. Rev. B **89**, 144502 (2014).
[4] M. N. Gastiasoro and B. M. Andersen, Phys. Rev. **92** 140506 (2015).
[5] V. Cvetkovic and O. Vafek, Phys. Rev. B **88**, 134510 (2013).
[6] R. M. Fernandes, S. A. Kivelson, E. Berg, arXiv:1504.03656 (unpublished).
[7] Avci *et al.* Phys. Rev. B **88**, 094510 (2013).
[8] Böhmer *et al.* Nature Comm. **6**, 7911 (2015).
[9] Avci *et al.* Nature Comm. **5**, 3845 (2014).
[10] Wang *et al.* arXiv:1510.03685 (unpublished).